4-2009

Influence of Flanking Sequence Context on the Conformational Flexibility of Aminofluorene-Modified dG Adduct in dA Mismatch DNA Duplexes

Nidhi Jain

Srinivasarao Meneni

Vipin Jain
University of Rhode Island, vipinj_11@yahoo.co.in

Bongsup P. Cho
University of Rhode Island, bcho@uri.edu

Citation/Publisher Attribution

Nidhi Jain, Srinivasarao Meneni, Vipin Jain, Bongsup P. Cho; Influence of flanking sequence context on the conformational flexibility of aminofluorene-modified dG adduct in dA mismatch DNA duplexes, *Nucleic Acids Research*, Volume 37, Issue 5, 1 April 2009, Pages 1628–1637, https://doi.org/10.1093/nar/gkn1063
Available at: http://dx.doi.org/10.1093/nar/gkn1063

Influence of Flanking Sequence Context on the Conformational Flexibility of Aminofluorene-Modified dG Adduct in dA Mismatch DNA Duplexes

1628–1637 *Nucleic Acids Research, 2009, Vol. 37, No. 5* *Published online 16 January 2009*
doi:10.1093/nar/gkn1063

Influence of flanking sequence context on the conformational flexibility of aminofluorene-modified dG adduct in dA mismatch DNA duplexes

Nidhi Jain, Srinivasarao Meneni, Vipin Jain and Bongsup P. Cho*

Department of Biomedical and Pharmaceutical Sciences, College of Pharmacy, University of Rhode Island, Kingston, RI 02881, USA

Received October 16, 2008; Revised December 8, 2008; Accepted December 16, 2008

ABSTRACT

When positioned opposite to a dA in a DNA duplex, the prototype arylamine–DNA adduct [*N*-(2′-deoxyguanosin-yl)-7-fluoro-2-aminofluorene (FAF)] adopts the so-called 'wedge' (W) conformation, in which the carcinogen resides in the minor groove of the duplex. All 16 FAF-modified 12-mer *N*GN*/*NAN* dA mismatch duplexes (G* = FAF, *N* = G, A, C, T) exhibited strongly positive induced circular dichroism in the 290–360 nm range ($ICD_{290–360\,nm}$), which supports the W conformation. The $ICD_{290–360\,nm}$ intensities were the greatest for duplexes with a 3′-flanking T. The AG**N* duplex series showed little adduct-induced destabilization. An exception was the AG*T duplex, which displayed two well-resolved signals in the ^{19}F NMR spectra. This was presumably due to a strong lesion-destabilizing effect of the 3′-T. The flanking T effect was substantiated further by findings with the TG*T duplex, which exhibited greater lesion flexibility and nucleotide excision repair recognition. Adduct conformational heterogeneity decreased in order of TG*T > AG*T > CG*T > AG*A > AG*G > AG*C. The dramatic flanking T effect on W-conformeric duplexes is consistent with the strong dependence of the $ICD_{290-360}$ on both temperature and salt concentration and could be extended to the arylamine food mutagens that are biologically relevant in humans.**

INTRODUCTION

Arylamine carcinogens are among the most notorious environmental carcinogens (1). Arylamine–DNA adducts have been detected in various human tissues and thus have been implicated in the etiology of human cancers (2,3). It is important to resolve the structural and conformational properties of arylamine–DNA adducts in order to elucidate the mechanisms by which bulky adducts are accommodated by repair proteins and polymerases (4).

The most persistent and major adduct generated by the environmental arylamine carcinogen 2-aminofluorene is the *N*-deacetylated adduct [*N*-(2′-deoxyguanosin-yl)-2-aminofluorene (AF)] (Figure 1a) (5,6). The mutational and repair characteristics of AF have been shown to be highly dependent on sequence context and the type of cells employed (7,8). Fully paired AF-modified DNA duplexes are known to exist in sequence dependent equilibrium between external B-type (B) and stacked (S) conformations with an exchange time in the millisecond range (Figure 1b) (9–13). A similar S/B conformational heterogeneity has been observed with the food-borne heterocyclic arylamine mutagen 2-amino-l-methyl-6-phenylimidazo[4,5-*b*]pyridine (PHIP) (14). A large planar aminopyrene (AP) adduct derived from the environmental mutagen 1-nitropyrene adopts the S-conformer exclusively (15,16). In contrast, the small, non-planar aminobiphenyl (ABP) adduct derived from the human bladder carcinogen 4-ABP adopts predominantly the B-conformer (17). These findings provide strong evidence for the importance of the planarity of carcinogens in determining S/B heterogeneity (9,10).

The so-called 'wedge' (W) conformation predominates in those DNA duplexes in which AF-modified dGs mispair with dAs at the lesion site (18). Such a configuration forces the hydrophobic aminofluorene to be positioned within the narrow minor groove. At neutral pH, there is evidence of hydrogen bonds stabilizing the (syn)dG*:(anti)dA mispair. At acidic pH, however, the protonated N1 of dA forms a single hydrogen bond with O^6-dG*, thus displacing the carcinogen further away from the helix axis relative to its position under neutral pH conditions (19). Similar situations have been observed

*To whom correspondence should be addressed. Tel: +1 401 874 5024; Fax: +1 401 874 5766; Email: bcho@uri.edu

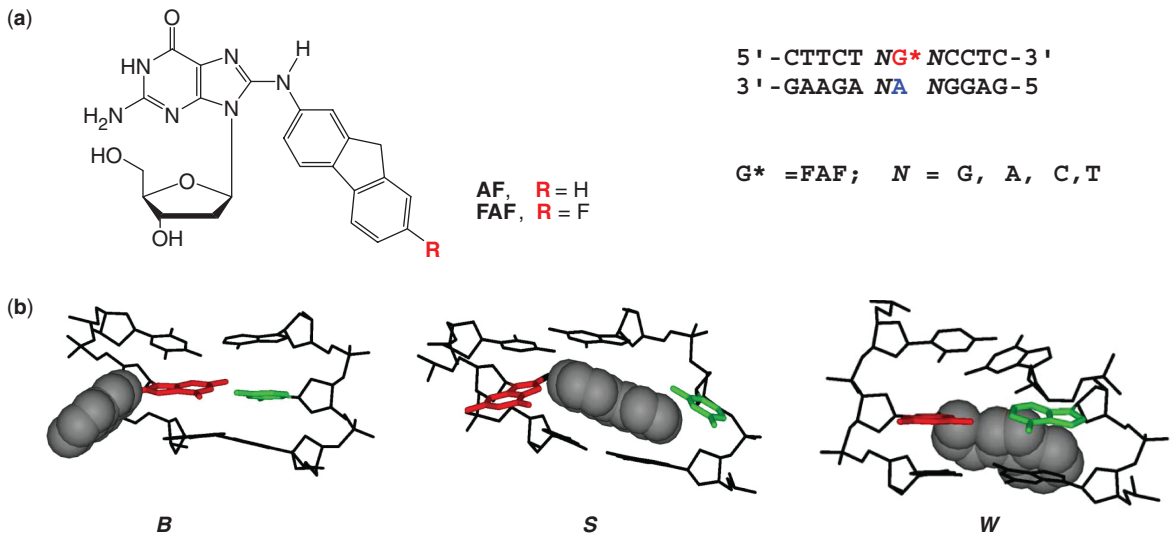

Figure 1. (**a**) Chemical structures of dG-C8 aminofluorene adducts and 12-mer DNA sequence contexts used in the present study. AF, *N*-(2′-deoxyguanosin-8-yl)-2-aminofluorene; FAF, *N*-(2′-deoxyguanosin-8-yl)-7-fluoro-2-aminofluorene. (**b**) The major groove views for AF-induced conformational motifs in duplex DNA: B (B-type), S (stacked), and W (wedge) conformers. The modified dG and the complementary (dC for B and S, and dA for W) are indicated with red and green lines, respectively, and the carcinogenic aminofluorene is highlighted with grey CPK. Hydrogen atoms are not shown for visual clarity.

with dG or dI situated opposite to this lesion (20). Modeling studies indicate that both ABP and AP can also exist in the W-conformation (21), favoring G→T transversions, the most targeted point mutations by these bulky carcinogens (7,8). Stone and coworkers have shown that the food mutagen 2-amino-3-methylimidazo[4,5-*f*]quinoline (IQ) positioned at G3 in the *NarI* sequence (5′-CG1G2CG3CC-3′) adopts an S-like conformation (22,23). In contrast, G1- and G2-IQ adducts adopt a W-like conformer, in which the isoquinoline moiety is pushed further into the minor groove (24). These prior findings suggest that helix intercalation is favored when both the 5′- and 3′-flanking nucleotides in the complementary strand are dGs. Zalizniak *et al.* (25) have reported that the minor (<15%), but most persistent, N^2-AAF [3-(2′deoxyguanosin-N^2-yl)-2-acetylaminofluorene] adduct maintains a right-handed helix with Watson–Crick base pairing throughout the duplex including across the lesion site. Such a configuration allows the carcinogen moiety to be sandwiched tightly by the walls of the minor grove, resulting in an unusually stable duplex molecule ($\Delta T_m + 6.2^\circ$C; $\Delta\Delta G - 1.8$ kcal/mol) (25).

We have previously examined the mutagenic relevance of the AF-induced S/B/W-heterogeneity in translesion DNA synthesis by dynamic circular dichroism (CD)/^{19}F nuclear magnetic resonance (NMR) and differential scanning calorimetry (DSC) (26–29). The results indicated that the steric free B-conformer accommodates a correct dCTP resulting in either a faithful replication or deletion mutations via a slippage mechanism. However, existence of the S-conformer could lead to a thermodynamically stable W-conformeric dG*:dA mispair at the lesion site. The rate and fidelity of nucleotide insertion opposite the modified base has been shown to be governed both by flanking sequence context and nature of polymerase, which determines the balance between kinetic and thermodynamic effects (30). Microcalorimetry studies showed little thermodynamic preference ($\Delta\Delta G^\circ$ ~0 kcal/mol) for insertion of dCTP over dATP opposite to the AF-adduct (29), rationalizing a wide range (2–59%) of sequence-dependent G-T mutational specificity in COS cells (7). During replication elongation, the carcinogen in the minor groove imposes a steric burden in the DNA-binding area of a polymerase, consequently reducing the rate of nucleotide insertion at several 5′ downstream bases (26).

Although extensive studies have examined sequence effects of AF-induced S/B equilibrium (9–13), very little is known about sequence effects on the W-conformation. In the present study, we investigated sequence effects on W-conformeric DNA duplexes by dynamic CD and ^{19}F NMR spectroscopy. To this end, we prepared 16 12-mer *N*G**N*/*N*A*N* duplexes (5′-CTTCT*N***G***N*CCTC-3′:5′-GAGG*N*A*N*AGAAG-3′, G* = FAF) (Figure 1a), in which the fluorinated AF lesion (FAF) was mispaired with dA and the flanking sequences were systematically varied (*N* = G, A, C, T). We determined the conformation adopted by the dA mismatch duplexes and their relative lesion conformational flexibilities.

EXPERIMENTAL SECTION

Crude oligodeoxynucleotides in 10–15 μmol scales in desalted form were obtained from Sigma-Genosys (The Woodlands, TX). All high performance liquid chromatography (HPLC) solvents were purchased from Fisher Inc. (Pittsburgh, PA). (Caution: 2-Aminofluorene derivatives are mutagens and suspected human carcinogens and therefore must be handled with caution).

The model sequence systems

Following the published procedures (11,13), we prepared four sets of 12-mer oligonucleotides (namely, GG*N* series, d[CTTCT**GG***N***CCTC]; AG*N* series, d[CTTCT **AG***N***CCTC]; CG*N* series, d[CTTCT**CG***N* CCTC]; and TG*N* series, d[CTTCT**TG***N***CCTC];), in which the FAF-modified guanines (G*) are flanked by four natural bases (*N* = G, A, C, T] (Figure 1a, see also Supplementary Table S1 for complete duplex sequences). The HPLC system consisted of a Hitachi EZChrom Elite unit with a L2450 diode array as a detector and employed a Waters XTerra MS C18 column (10 × 50 mm, 2.5 μ) with a 60-min gradient system involving 3–15% acetonitrile in pH 7.0 ammonium acetate buffer (0.10 M) with a flow rate of 2.0 ml/min. Characterization of FAF-modified AG*N* and CG*N* sequences have already been reported (13). The FAF-modified GG*C and TG*T sequences were characterized similarly by analyses of their UV and enzyme-digests/ESI-TOF-MS characteristics in the negative mode and the experimental details are described in Supplementary Figures S1 and S2. All the purified sequences were annealed with appropriate 12-mer complementary strand [d(GAGG*NAN*AGAAG)] to produce the desired dA-mismatched duplexes (Figure 1a). An identical set of 16 unmodified duplexes was also prepared as controls.

UV-melting experiments

UV-melting data were obtained using a Beckman DU 800 UV/VIS spectrophotometer equipped with a six-chamber, 1 cm path-length T_m cell. Sample cell temperatures were controlled by a Peltier temperature controller. Duplexes with a total concentration in the range of 0.2–14 μM were prepared in solutions containing 0.2 M NaCl, 10 mM sodium phosphate, and 0.2 mM EDTA at pH 7.0. Thermomelting curves were constructed by varying the temperature of the sample cell (1°C/min) and monitoring the absorbance of the sample at 260 nm. A typical melting experiment consisted of forward/reverse scans and was repeated three times. Thermodynamic parameters were calculated using the program MELTWIN® version 3.5 as described previously (11).

CD experiments

CD measurements were conducted on a Jasco J-810 spectropolarimeter equipped with a Peltier temperature controller. Typically, 2 ODS of each strand were annealed with an equimolar amount of a complementary sequence. The samples were dissolved in 400 μl of a neutral buffer (0.2 M NaCl, 10 mM sodium phosphate, 0.2 mM EDTA) and placed in a 1 mm path-length cell. The samples were heated at 85°C for 5 min and then cooled to 15°C over a 10 min period to ensure complete duplex formation. Spectra were acquired every 0.2 nm with a 2 s response time from 200 to 400 nm at a rate of 50 nm/min and were the averages of 10 accumulations and smoothed using 17 point adoptive smoothing algorithms provided by Jasco. For salt experiments, CD spectra were recorded at 15°C with increasing amount of NaCl: 0.2, 0.5, 1.0, 2.0, 3.0 and 5.0 M.

NMR experiments

Approximately 20–60 ODS of pure modified oligonucleotides were annealed with equivalent amount of complementary sequences to produce the corresponding 12-mer dA mismatch duplexes. The duplex samples were ultracentrifugated using a Pall Microsep MF centrifugal device (Yellow, MW cutoff = 1000). The centrifuged samples were dissolved in 300 μl of a neutral buffer (10% D_2O/90% H_2O containing 100 mM NaCl, 10 mM sodium phosphate and 100 μM tetrasodium EDTA, pH 7.0) and filtered into in a Shigemi tube through a 0.2 μm membrane filter for NMR experiments.

All ^1H and ^{19}F NMR results were recorded using a dedicated 5 mm $^{19}F/^1H$ dual probe on a Bruker DPX400 Avance spectrometer operating at 400.0 and 376.5 MHz, respectively. Imino proton spectra were obtained using phase sensitive jump-return sequences at 5°C and referenced relative to DSS. ^{19}F NMR spectra were acquired in the ^1H-decoupled mode and referenced to $CFCl_3$ by assigning external hexafluorobenzene in C_6D_6 at − 164.90 ppm. One-dimensional ^{19}F NMR spectra were measured between 5°C and 60°C with increment of 5–10°C. Additional temperatures were used as needed to clarify signal exchange process (Supplementary Figure S3). Temperatures were maintained by a BRUKER-VT unit by adding liquid N_2 to the probe. Spectra were obtained by collecting 65 536 points using a 37 664 Hz sweep width and a recycle delay of 1.0 s. A total of 1600 scans were acquired for each dynamic NMR spectrum. All FIDs were processed by zero-filling, exponential multiplication using a 20 Hz line broadening factor and Fourier transformation. NOESY/exchange ^{19}F NMR spectra were obtained in the phase-sensitive mode using the following parameters: sweep width 4529 Hz, number of complex data points in t_2 1024, number of complex FIDs in t_1 256, number of scans 96, dummy scans 16, recycle delays 1.0 s and mixing time 400 ms. The data were apodized with sine function using 2 Hz line broadening in both dimensions and Fourier transformed with the 1024 × 256 data matrix.

RESULTS

$ICD_{290–360\,nm}$ of the *N*G*N*/*N*A*N* mismatch duplexes

Figure 2 shows CD overlays of the FAF-modified dA mismatch duplexes in four series: (a) GG*N*, (b) AG*N*, (c) CG*N* and (d) TG*N* (*N* = G, A, C T). All of the *N*G*N*/*N*A*N* duplexes exhibited very strongly positive induced CD in the 290–360 nm range ($ICD_{290–360\,nm}$). This is in contrast with the unmodified control duplexes which showed no such $ICD_{290–360\,nm}$ (11). We have shown previously that positive $ICD_{290–360\,nm}$ is indicative of a S- or W-conformation, whereas negative $ICD_{290–360\,nm}$ is indicative of a B-type conformation (27). The intense positive $ICD_{290–360\,nm}$ values observed for the *N*G*N*/*N*A*N* duplexes were sequence dependent, presumably due to varied interactions of the carcinogen with

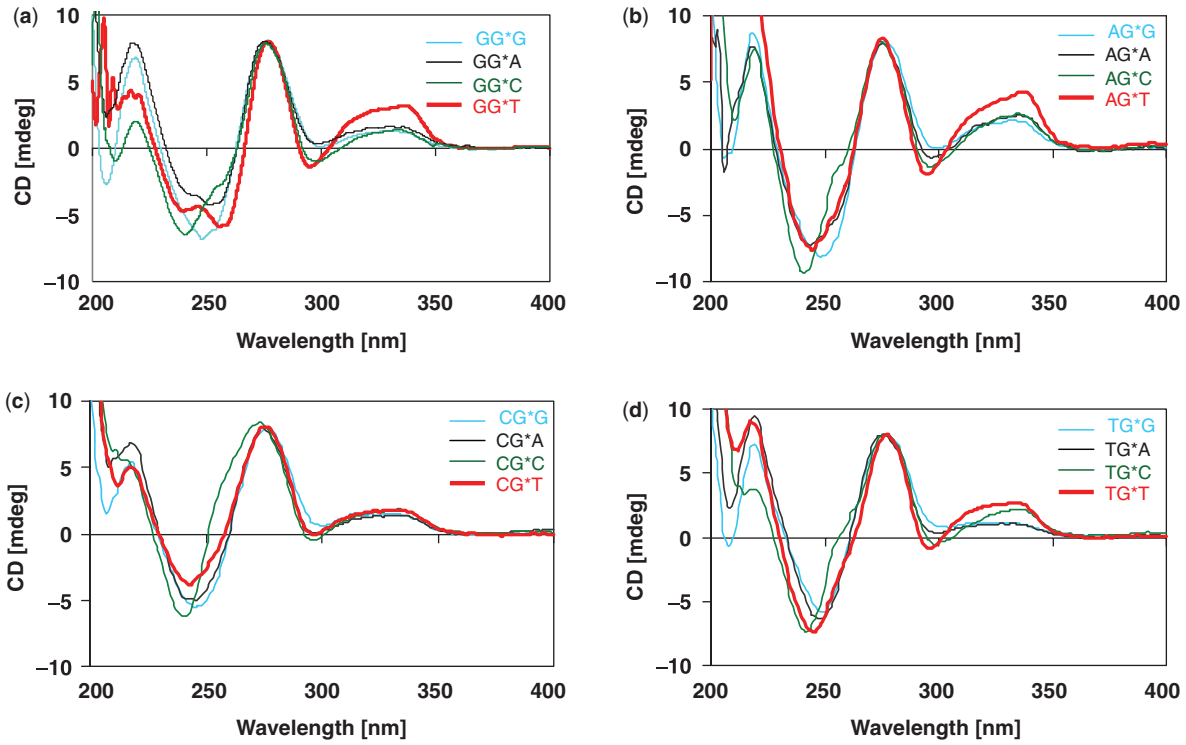

Figure 2. CD spectral overlays of the FAF-modified duplexes in the 200–400 nm range at 15°C for (**a**) the GG*N*, (**b**) AG*N*, (**c**) CG*N* and (**d**) TG*N* duplex series.

W-conformer minor groove chiral DNA. With the exception of the CG*T duplex (Figure 2c), the extent of positive $ICD_{290–360\,nm}$ of duplexes with a 3′-T was significantly greater than that observed for other duplexes within the same series.

Temperature dependent $ICD_{290–360\,nm}$ of the AG*N, CG*T and TG*T dA mismatch duplexes

As shown in Figure 3a, variation was observed in the $ICD_{290–360\,nm}$ of the AG*N, CG*T and TG*T duplexes in the 5–35°C range. The isomeric AG*C and AG*G duplexes showed little change in $ICD_{290–360\,nm}$, whereas those with a flanking T (AG*T, CG*T and TG*T) exhibited greater temperature dependence. The temperature/$ICD_{290–360\,nm}$ effect decreased in order of TG*T > AG*T > CG*T > AG*A > AG*C ~ AG*G. The large temperature dependence of $ICD_{290–360\,nm}$ intensity provides evidence of an effect of the flanking T on the conformational flexibility of W-conformer duplexes (27).

Salt-dependent $ICD_{290–360\,nm}$ of the AG*N, CG*T and TG*T dA mismatch duplexes

Mismatch duplexes were exposed to a range of salt concentrations to assess conformational flexibility at the lesion site. Figure 3c shows overlays of CD spectra of the AG*N, CG*T and TG*T duplexes in solutions of increasing ionic strength. The $ICD_{290–360\,nm}$ of all of the mismatch duplexes, except for AG*C and CG*T, decreased steadily with increasing salt concentration (0.2–5.0 M NaCl). The results indicate gradual conformational disturbance of the lesion structure and the trend is generally consistent with the temperature dependent CD experiments and the dynamic ^{19}F NMR results (see below).

Duplex stability

Both FAF-modified and control duplexes exhibited UV melting profiles that were characteristic of a monophasic, sigmoidal, helix-coil transition. Thermal and thermodynamic parameters were obtained by van't Hoff analyses as described previously (11) and the results are shown in Table 1. The T_m and $\triangle G^\circ$ values of the AG*N, CG*T and TG*T duplexes were found to be comparable to those of the control duplexes. The lack of noticeable adduct-induced duplex destabilization is most likely due to van der Waals' interactions between the carcinogen moiety and surfaces in the minor groove (26). This is in contrast to the S/B conformeric DNA duplexes, which induces thermodynamic destabilization as a result of loss of Watson–Crick base pairs (S-conformer) or unfavorable carcinogen-solvent interactions (B-conformer) (11). The T_m values of the chemically isomeric AG*A, AG*T and TG*T duplexes varied (43.6°C, 41.9°C and 39.2°C, respectively), evidencing the importance of flanking base polarity (A:T versus T:A). The T_m results from the UV melting data tend to be more sensitive to the overall T_m, while the dynamic NMR described below represents a localized melting, whose effect would be minimized in longer duplexes.

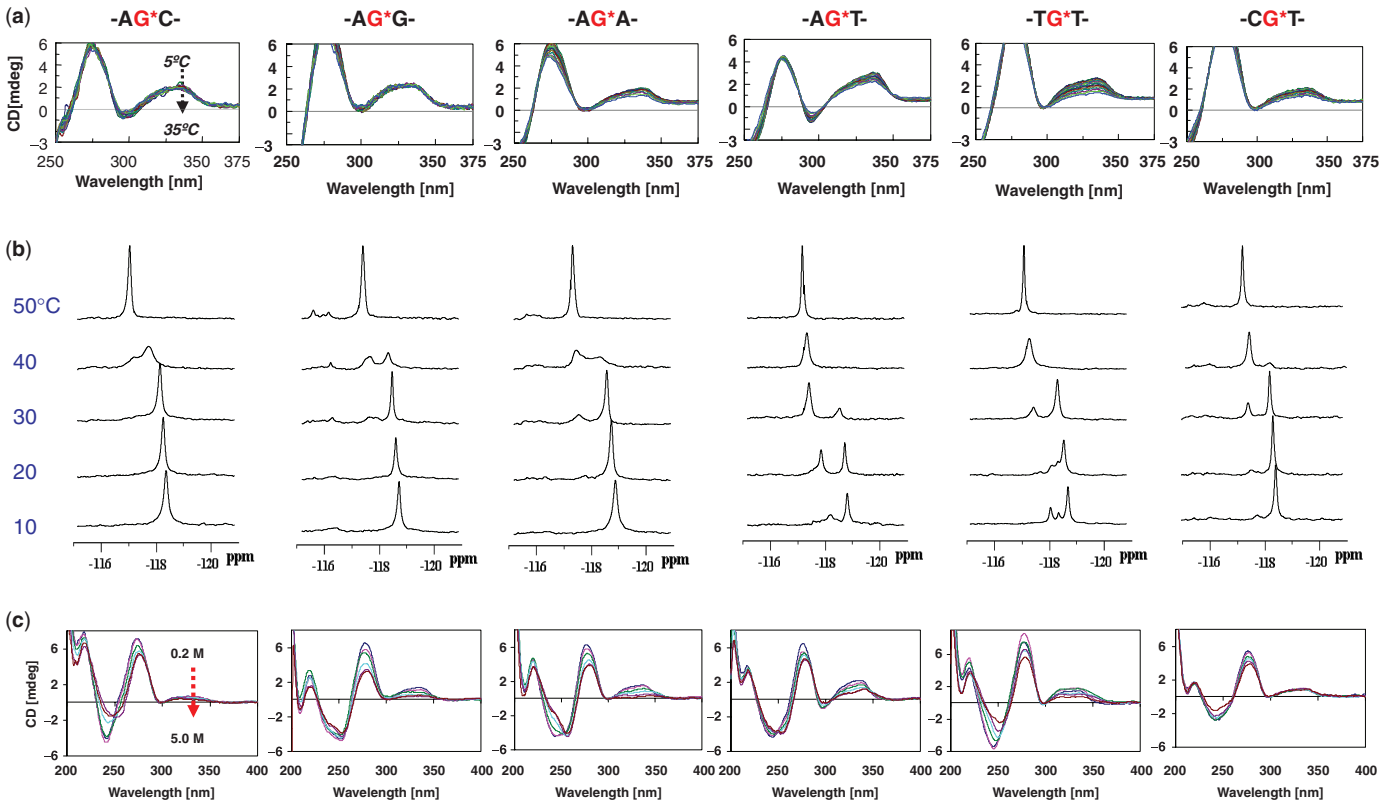

Figure 3. (**a**) Temperature dependent CD spectra of -AG*N*-, -TG*T- and -CG*T- dA mismatch duplexes (G* = FAF-adduct, *N* = G, A, C, T) (see Figure 1 for full sequence). Dotted arrows denote increasing temperatures from 5 to 35°C. (**b**) Dynamic ^{19}F NMR spectra (−115 to −121 ppm) of the -AG*N*-, -TG*T- and -CG*T- dA mismatch duplexes. Spectra of all sequences were shown in five standard temperatures: 10, 20, 30, 40 and 50°C (see Supplementary Figure S3 for full temperature ranges). (**c**) CD spectral overlays of the FAF-modified duplexes at 15°C. Dotted arrows denote increasing NaCl concentration: 0.2, 0.5, 1.0, 2.0, 3.0 and 5.0 M.

Table 1. Thermodynamic parameters for the FAF-modified AG*N, TG*T and CG*T dA mismatch duplexes

Sequence[a]	$-\Delta G^{b}$ (kcal/mol)	$-\Delta H^{b}$ (kcal/mol)	T_m[c] (°C)	$\Delta\Delta G^{d}$ (kcal/mol)	$\Delta\Delta H^{e}$ (kcal/mol)	ΔT_m[f] (°C)
-AG*G/CAT-	9.3 (9.0)[g]	74.9 (68.5)	48.3 (48.5)	−0.3	−6.4	−0.2
-AG*A/TAT-	7.7 (7.9)	59.6 (75.5)	43.6 (43.1)	0.2	15.9	0.5
-AG*C/GAT-	8.4 (9.7)	47.0 (81.5)	50.2 (49.6)	1.3	34.5	0.6
-AG*T/AAT-	7.4 (7.8)	59.3 (70.5)	41.9 (42.6)	0.4	11.2	−0.7
-TG*T/AAA-	7.0 (6.6)	74.6 (68.7)	39.2 (37.5)	−0.4	−5.9	1.7
-CG*T/AAG-	8.1 (8.6)	62.8 (78.4)	47.1 (47.8)	0.5	15.6	−0.7

[a]The central trimer portion of the 12-mer duplex (G* = FAF-adduct). See Table S1 for full sequence details.
[b]The results of curve fit and T_m–lnCt dependence were within ±15% of each other and therefore these numbers are average of the two methods. The average standard deviations for $-\Delta G^{\circ}$ and $-\triangle\Delta H^{\circ}$ are ±0.22 and ±6.33, respectively.
[c]T_m values at 14 mM taken from the $1/T_m - \ln Ct/4$.
[d]$\Delta\Delta G = \Delta G$ (FAF−modified duplex) $-\Delta G^{\circ}$ (control duplex).
[e]$\Delta\Delta H = \Delta H^{\circ}$ (FAF-modified duplex) $-\Delta H^{\circ}$ (control duplex).
[f]ΔTm = T_m (FAF-modified duplex) $-T_m$ (control duplex).
[g]Data in parentheses are from unmodified control duplexes.

Dynamic ^{19}F NMR spectra

Although powerful, obtaining ^{19}F NMR spectra of a series of duplex samples is an enormous undertaking (11–13,26–28). Therefore, our focus was placed initially on a small group of selected sequences, namely a series of four AG*N duplexes. The TG*T and CG*T duplexes were added subsequently to further investigate the conformational effect of flanking T (see below). Figure 3b shows dynamic ^{19}F NMR spectra of the six FAF-duplexes in the 10–50°C range (see Supplementary Figure S3 for full temperature ranges). These duplexes could be grouped into two categories on the basis of their isomeric status: (a) AG*C, AG*G and CG*T; (b) AG*A, AG*T and TG*T.

*AG*C and AG*G*. The AG*C and AG*G dA mismatch duplexes are chemically isomeric with each other, differing only in the polarity of their 3′-flanking base pair (G:C versus C:G). The dynamic NMR profiles of the two duplexes produced similar single persistent signal below 30°C. These signals exhibited significant H/D isotope effects (0.17 and 0.24 ppm at 20°C for the AG*G and AG*C duplexes, respectively). The ^{19}F resonance of the exposed FAF residue in a B- or W-conformer has been shown to be more susceptible to solvent-induced shielding (usually >0.2 ppm) than the buried FAF in the S conformer (usually < 0.1 ppm) upon increasing the deuterium content from 10% to 100% (13,26). These NMR results, coupled with the strong positive $ICD_{290–360\,nm}$ (Figure 2, described above), provide evidence for the presence of a stable W-conformation, in which FAF is partially exposed in the minor groove. The imino proton spectra of the AG*C and AG*G duplexes at 5°C showed well-resolved signals, consistent with a single conformation. The stable W-conformeric ^{19}F NMR signals underwent duplex melting in the 35–40°C range, coalesced around 45°C and eventually narrowed at 50°C as the duplexes denatured into FAF-modified single strands. The NMR and salt-dependency CD results demonstrated that the AG*G duplex exhibits slightly greater conformational heterogeneity than the AG*C duplex (Figure 3).

*AG*A and AG*T*. The isomeric AG*A and AG*T duplexes showed significant H/D isotope effects (0.14 and 0.25 ppm at 20°C for the AG*A and AG*T duplexes, respectively) and positive $ICD_{290–360\,nm}$ intensities, both of which are characteristic of the W-conformation (26,27). However, it was noted that the AG*A and AG*T pair exhibited generally greater conformational heterogeneity than the AG*C and AG*G isomeric pair, especially at lower temperatures (Figure 3b). These results indicate that an A:T flanking base pair has greater influence on conformational flexibility at the lesion site than a G:C flanking base pair.

The AG*T duplex showed markedly greater conformational heterogeneity than the AG*A duplex as evidenced by its two well resolved signals at 20°C (Figure 3b). Meanwhile, the NOESY spectrum of the AG*T duplex (data not shown) failed to yield any discernable off-diagonal cross-peaks at 20°C, suggesting that no chemical exchanges occurred. This is contrasted to the S/B conformeric exchange of the corresponding AG*T dC match duplex, which showed well-defined exchangeable contours (13,26). The shape and chemical shifts of the upfield W-conformer signal at –118.8 ppm did not change appreciably until the temperature was brought to 30°C; it then proceeded to collapse quickly in the narrow 30–35°C range. The dynamic NMR results are consistent with the strong temperature and salt-dependent CD findings (Figure 3a and c, respectively) and can be considered to be a non-exchangeable W- to B-transition rather than an S/B dynamic exchange typically observed for fully paired dC match duplexes. The greater heterogeneity of AG*T relative to AG*A is a clear indication of the impact of 3′-T:A over 3′-A:T on W-conformer stability.

*TG*T duplex*. To substantiate the destabilizing flanking T effect, we conducted ^{19}F NMR analysis of the TG*T dA mismatch duplex in which the lesion was flanked by T on both sides. The $ICD_{290–360\,nm}$ of the TG*T duplex was strongly positive as expected for the W-conformation. The TG*T duplex exhibited at least three ^{19}F signals of varying intensity, all of which interchanged with one another (NOESY) (Figure 4). This could be interpreted as evidence of an S/B/W equilibrium. Specifically, the highest, most upfield signal at 5°C, −118.8 ppm, could be assigned to the W-conformer and the remaining signals, −118.0 and −118.4 ppm, as the B- and S-conformers, respectively. At 25°C, the B/S signals started to coalesce with the major W-conformeric signal at −117.3 ppm (Figure 3b and Supplementary Figure S3). This W-signal remained steady until the temperature reached 40°C, at which time it underwent a typical exchange process with a denatured signal at 40°C. Furthermore, the imino proton spectrum exhibited complex proton signals with varying degrees of intensity indicative of a mixture of conformers (Supplementary Figure S4). Given the isomeric nature of the AG*A, AG*T and TG*T duplexes, the dramatic heterogeneity observed for the TG*T duplex must be due to the 5′-flanking T. The progressive nature of decreasing conformational heterogeneity among the isomers (TG*T > AG*T > AG*A) indicates the critical role of flanking T on both sides (3′ and 5′) of the lesion. The effect of base polarity (T:A versus A:T) is clear especially when the dynamic ^{19}F NMR profiles of the isomeric TG*T and AG*A duplexes are compared (Figure 3b).

*CG*T duplex*. The CG*T duplex is chemically isomeric to the AG*C and AG*G duplexes, with a unique flanking base arrangement. As shown in Figure 3, the conformer heterogeneity profile of CG*T exists in between those of AG*A and AG*T. The imino proton spectrum at 5°C (Supplementary Figure S4) showed well-resolved signals, indicating presence of a single W-conformation at lower temperature. The major signal exhibited an H/D isotope shift of 0.3 ppm at 20°C as expected for a W-conformation (Supplementary Figure S5). The intermediacy of CG*T is not surprising given that the lesion is flanked by a stabilizing C:G pair and a destabilizing T:A pair on the 5′ and 3′-sides, respectively. Thus while both AG*T and CG*T are flanked by a 3′-T, a change of

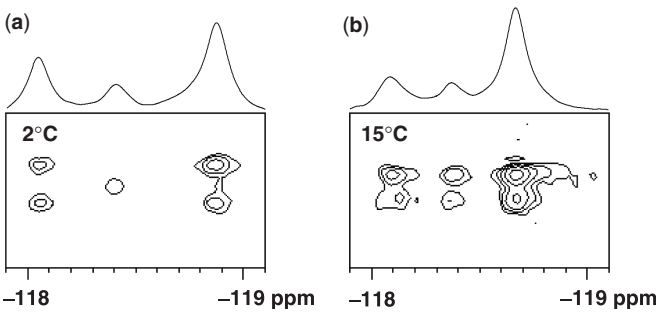

Figure 4. Temperature-dependent ^{19}F NMR NOESY spectra of the TG*T/AAA duplex recorded in 10% D_2O/90% H_2O pH 7.0 buffer at (**a**) 2°C and at (**b**) 15°C.

5′-A to 5′-C imparts greater conformational stability. Taken together, it can be concluded from these results that conformational flexibility decreases in order of flanking T:A >>> A:T > G:C > C:G on both sides (3′, 5′) of the lesion.

Comparison of dA-mismatch versus dC-match duplexes. Figure 5 compares ^{19}F NMR spectra of the dA-mismatch duplexes recorded in the present study with their normal dC-match counterparts at 20°C. As stated above, mismatch duplexes in general afforded a single major ^{19}F signal and a positive $ICD_{290–360\,nm}$, strong evidence for the presence of the W-conformation. Notable exceptions were the TG*T and AG*T duplexes, which exhibited multiple signals at lower temperatures, presumably due to a complex S/B/W-conformational heterogeneity. This is contrasted to the corresponding dC-match duplexes, which have been shown to exist in a well-defined, sequence-dependent conformeric mixture of B and S (11,13). The W-conformeric signals were generally comparable or slightly shifted downfield (−118 to −119 ppm) to that of the S-conformer, indicating the similarity of their shielding environment, i.e. base-displacement and minor groove for S and W, respectively. The effect of flanking T on the lesion conformational flexibility was particularly prominent for mismatch duplexes (i.e. AG*T and TG*T).

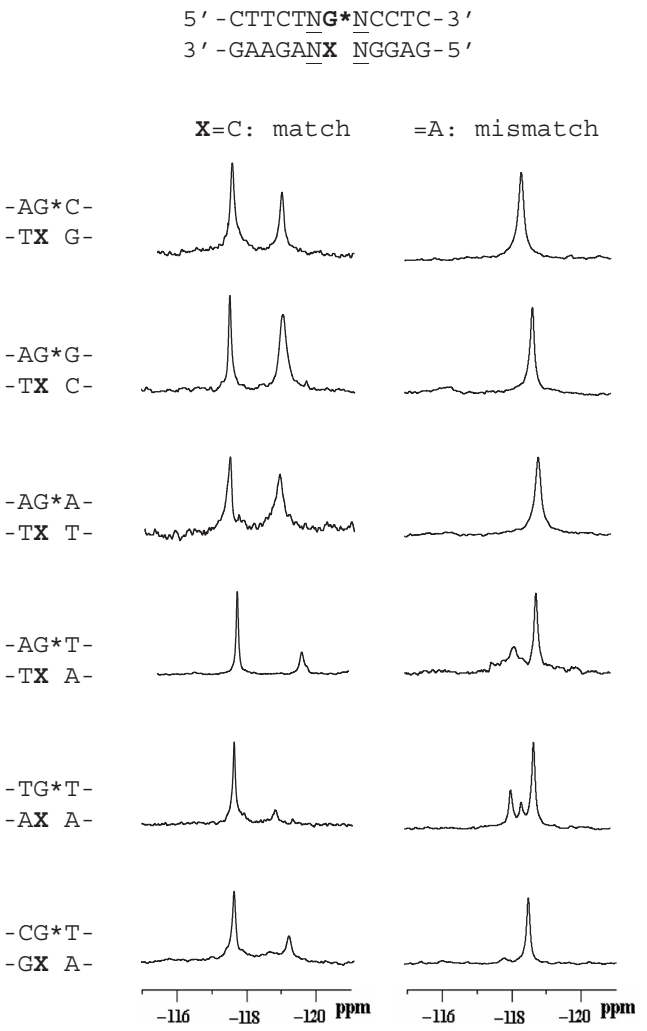

Figure 5. Comparison of ^{19}F NMR spectra of FAF-modified AG*N, TG*T and CG*T match (**X** = C) duplexes with the corresponding mismatch (**X** = A) series.

DISCUSSION

All 16 of the examined *N*G*N*/*N*A*N* dA mismatch duplexes (Figure 2) exhibited a positive ellipticity in the range of 290–360 nm ($ICD_{290–360\,nm}$). This is a strong indication for adoption of the W-conformation, in which the carcinogen moiety resides in the narrow minor groove region (27). Sequence dependence of $ICD_{290–360\,nm}$ intensity was also demonstrated. Of particular importance was the unusually intense $ICD_{290–360\,nm}$ produced by the sequences with a 3′-flanking T (with the exception of CG*T, Figure 2c) in all of the *N*G*N* duplex series. The dynamic ^{19}F NMR experiments conducted on several selected duplexes provided additional evidence of this flanking sequence effect. The AG*N duplex series all gave a single major ^{19}F signal in the −118 to −119 ppm range at 5°C with minimal alteration in duplex stability (ΔT_m −0.7 to +0.6°C; $\Delta\Delta G$ −0.3 to +0.4, Table 1). Meanwhile, the corresponding dC match AG*N duplexes exhibited S/B equilibriums with significant adduct-induced duplex destabilization (ΔT_m −6.3 to −10.7°C; $\Delta\Delta G$ + 2.1 to + 2.8 kcal/mol) (11,13). On comparison, effect of flanking T on the lesion conformational flexibility was particularly prominent for mismatch duplexes (i.e. AG*T and TG*T) (Figure 5).

The dynamic ^{19}F NMR profiles (Figure 3b) demonstrate the importance of the nature and polarity of the flanking base pairs (A:T versus G:C) in determining lesion conformational stability. The isomeric AG*A and AG*T duplexes exhibited collectively greater conformational heterogeneity than the isomeric AG*G and AG*C duplexes. A significant base polarity effect was also observed. Thus, while the AG*G and AG*C duplexes had relatively similar ^{19}F NMR dynamic melting profiles, the AG*A and AG*T duplexes exhibited dramatic differences in this regard (Figure 3b). Conformational flexibility was found to be greatest for AG*T, which emphasizes the power of the flanking T effect. In line with this observation, the AG*T duplex exhibited the most dramatic $ICD_{290–360\,nm}$ effect as a function of both temperature and salt concentration (Figure 3a and c).

Dynamic ^{19}F NMR spectra of the TG*T duplex, in which the lesion is flanked by T on both sides, demonstrated that the duplex exhibited the most severe conformational flexibility of all duplexes examined; this pronounced flexibility is consistent with an S/B/W-equilibrium. The $ICD_{290–360\,nm}$/^{19}FNMR analysis of AG*T and TG*T duplexes led us to hypothesize that the greater the lesion conformational heterogeneity, the higher the $ICD_{290–360\,nm}$ intensity. To verify this, we obtained dynamic ^{19}F NMR of CG*T duplex, which unlike the rest of the 3′-T duplexes of *N*G*N* series

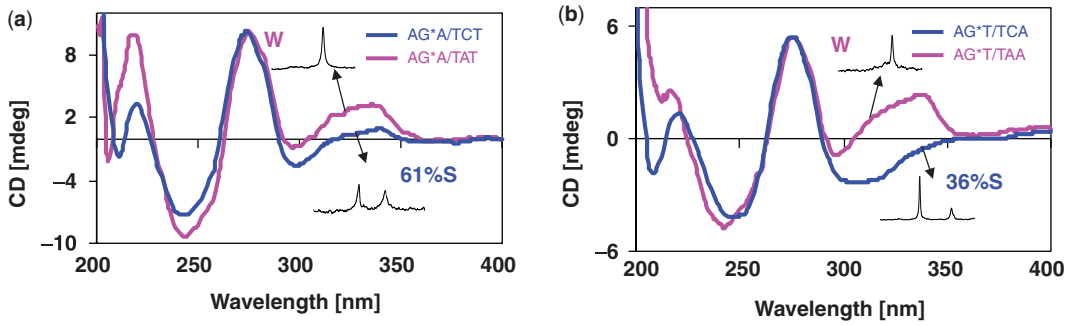

Figure 6. CD spectral overlays of the FAF-modified duplexes in the 200–400 nm range at 10°C for (**a**) AG*A/TCT, AG*A/TAT, and (**b**) AG*T/TCA, AG*T/TAA. The ^{19}F NMR results of the dC match duplexes give the relative populations of B and S conformers. The corresponding dA mismatch duplexes exist exclusively as W-conformers.

exhibited lower $ICD_{290–360\,nm}$. The results showed that the melting profile of the CG*T duplex was in between that of AG*A and AG*T. The enhanced stability of CG*T relative to AG*T and TG*T is governed by a 5′-C. Taken together, these results indicate that the stability of an FAF-induced W-conformation depends on the flanking base 3′ of the lesion, such that there is decreasing stability in the following order: C > G > A > T. A similar sequence effect was observed for the corresponding dC-match duplexes (13). While there are slight variations, a similar trend for a neighboring effect has also been observed for other duplexes containing mismatches and adducts (31). The dramatic effect of base polarity at the flanking position is clearly evident when the ^{19}F NMR melting profiles of the isomeric TG*T and AG*A duplexes are compared (Figure 3b).

The $ICD_{290–360\,nm}$ and ^{19}F NMR spectra of the dC-match and dA-mismatch duplexes in the AG*A and AG*T sequence contexts are shown together in Figure 6 to enable a visual comparison. Positive $ICD_{290–360\,nm}$ values are indicative of a S- or W-conformation, whereas negative $ICD_{290–360\,nm}$ values are associated with a B-type conformation (27). In both cases, the differences in $ICD_{290–360\,nm}$ are striking, in accordance with their conformational heterogeneity. The AG*A dA mismatch duplex adopted exclusively a W-conformation, whereas the corresponding dC match duplex adopted a 61%:39% mixture of S and B-conformers (13) (Figure 6a). Similarly, the AG*T dA mismatch duplex existed primarily in the W-conformation, whereas the corresponding dC match duplex adopted in a 36%:64% equilibrium of S and B-conformers (Figure 6b) (13). These examples demonstrate clearly the utility of the $ICD_{290–360\,nm}$/dynamic ^{19}F NMR patterns for probing arylamine-induced conformational heterogeneity.

BIOLOGICAL IMPLICATION

In the present model study we investigated the effects of sequence context on the conformational flexibility of DNA duplexes containing a G[FAF]: a mismatch base pair. Our data were acquired primarily in non-physiological conditions (i.e. buffer-only systems, low temperatures, no enzymes and proteins), and thus may be viewed of limited cellular relevance. However, adduct-induced conformational heterogeneity occurs in a millisecond time scale (13), and consequently the observed conformational effects could be localized in the active motifs of enzymes and recognition proteins, thereby providing valuable molecular insights on the efficiency of post-replication repair processes such as nucleotide excision repair (NER).

Adduct-induced conformational flexibility is greatly modulated by the type of base pair configuration and polarity flanking the lesion. This appears to be generally true for both match (13) and mismatch (present study) duplexes. We have shown previously that the presence of a purine base at the 3′-flanking position promotes S-conformation in the AF-adduct with greater efficiency in the UvrABC NER system in *E. coli* (12,13). The molecular basis for this novel 'conformation-specific NER' is not clear, even though available data points to the disruption of Watson–Crick bonds and base-displacement as major culprits.

Zou *et al.* (32) have shown that AF and AAF adducts in the TG*T sequence context are incised more efficiently in *E. coli* by a factor of 1.7 than in the CG*C context. It was argued that the T:A flanking base pairs in the former allow for local bend and flexibility, thus promoting greater conformational heterogeneity. Clearly, the weaker local base–base stacking interactions involving the TG* and G*T dinucleotides facilitated destabilization. In line with this finding, lower T_m and $-\Delta G^\circ$ values were observed for unmodified, as well as AF- (11) and FAF-modified TG*T (Table 1) duplexes. Figure 7 compares the ^{19}F NMR spectra of fully-paired FAF-modified 12-mer dC match duplexes in the CG*C and TG*T sequence contexts. The CG*C duplex exhibited an equal intensity of two well-resolved signals at −117.4 and −118.9 ppm, which correspond to the B- and S-conformer, respectively. In contrast, the TG*T duplex exhibited complex heterogeneities with what appears to be pseudo B-type conformers (labeled *). These NMR data support a linkage between the flanking T-induced lesion-conformational flexibility and repair susceptibility. Thus, NER recognition of the bulky AF-adduct involves not just thermodynamics and the quality of Watson–Crick base pairs, but also conformational flexibility and mobility at the lesion site.

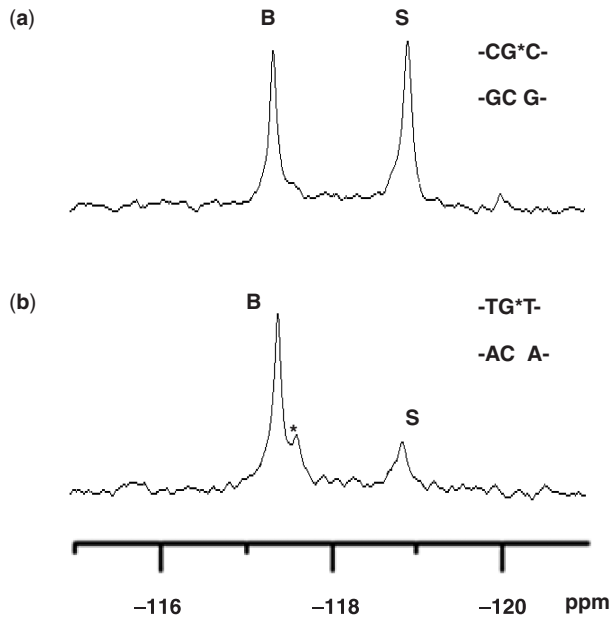

Figure 7. ^{19}F NMR spectra (−115 to 121 ppm) of (**a**) the CG*C and (**b**) TG*T match duplexes recorded at 20°C. Asterisk denotes an extra B-type conformation.

Similar 'flanking T-effects' have been reported for other lesions. For example, Geacintov and co-workers (33,34) have shown that the *trans-anti*-BP-dG adduct flanked by T (TG*T) existed in dynamically flexible multiple conformations, featuring more perturbed stacking interaction at the lesion site, whereas the same adduct in the CG*C context adopted a single minor groove conformation. The multi-conformeric TG*T duplex exhibited significantly lower T_m (−15°C) and was found to be more repair-prone by a factor of 2.3 than the CG*C duplex (33). Kalam *et al*. (35) have studied the replication of vectors modified by the oxidative damage lesions Fapy-dG and 8-oxo-dG in simian kidney (COS-7) cells. It was found that Fapy-dG was mutagenic, inducing primarily targeted G to T transversions and the mutational frequency was greater by a factor of 3.8 in the TG*T sequence relative to the CG*C context. 8-Oxo-dG, which was slightly less mutagenic than Fapy-dG, exhibited similar effect, i.e. 4-fold G to T transversions occurred in the 5′-TG*T sequence relative to TG*A. Molecular modeling showed that syn Fapy-dG:dATP pairing in the active site of pol β produces greater stacking in the TG*T sequence than in the TG*A sequence, thus leading to greater G to T efficiency. A similar stacking effect was observed for syn 8-oxo-dG (35). The same 8-oxo-dG afforded greater frequency of G to T transversions when it is adjacent to an abasic site, indicating the potential importance of tandem mutations (36).

It has been shown that the carcinogen moiety in the major groove of an AF-induced B-type conformer at the replication fork would reside in the solvent-exposed major groove of a template–primer DNA throughout the replication/translocation process (26). This is contrasted with the dA-mismatch W-conformer, in which the carcinogenic moiety in the minor groove would impose a major steric clash with the tight-packing amino-acid residues on the DNA-binding area of a replicative DNA polymerase (26). These results support a model in which adduct-induced conformational heterogeneities at positions remote from the replication fork affect polymerase function through a long-range DNA–protein interaction (27,37). The results in the present study were obtained in the duplex setting, and thus should be relevant to proofreading and/or NER of bulky lesions. Our structural data also provided valuable mutational insight as to how flanking sequences influence the lesion-induced conformational flexibility opposite dA at the replication fork.

In summary, we employed a combined $ICD_{290–360\,nm}$/^{19}F NMR procedure to study flanking sequence effects on AF-modified dA mismatch DNA duplexes. The nature of base pairs flanking the lesion and their polarity are important factors in determining the conformational flexibility of arylamine–DNA adducts (5′-T:A >> > A:T > G:C > C:G) when the affected base is mispaired with a dA. We also discussed the effect of the flanking T sequence on the lesion flexibility and mobility of W-conformeric DNA duplexes and its consequences on mutation and repair. The dramatic flanking T effect may be extended to the arylamine food mutagens that are biologically relevant in humans.

SUPPLEMENTARY DATA

Supplementary Data are available at NAR Online.

ACKNOWLEDGEMENTS

We thank Dr M. Paul Chiarelli for mass spectral measurements of the FAF-modified TG*T and GG*C sequences.

FUNDING

We are grateful to the National Institutes of Health (CA098296) for their financial support for this work. This research was also made possible in part by the use of the Rhode Island INBRE Research Core Facility, which is supported by the NCRR/NIH (P20 RR-16457). Funding for open access charge: National Institutes of Health (CA098296).

Conflict of interest statement. None declared.

REFERENCES

1. Talaska,G. (2003) Aromatic amines and human urinary bladder cancer: exposure sources and epidemiology. *J. Environ. Sci. Health C Environ. Carcinog. Ecotoxicol. Rev.*, **21**, 29–43.
2. Poirier,M.C. (2004) Chemical-induced DNA damage and human cancer risk. *Nature Rev. Cancer*, **4**, 630–637.
3. Feng,Z., Hu,W., Rom,W.N., Beland,F.A. and Tang,M.S. (2002) 4-Aminobiphenyl is a major etiological agent of human bladder cancer: evidence from its DNA binding spectrum in human p53 gene. *Carcinogenesis*, **23**, 1721–1727.
4. Guengerich,F.P. (2006) Interactions of carcinogen-bound DNA with individual DNA polymerases. *Chem. Rev.*, **106**, 420–452.
5. Heflich,R.H. and Neft,R.E. (1994) Genetic toxicity of 2-acetylaminofluorene, 2-aminofluorene and some of their metabolites and model metabolites. *Mutat. Res.*, **318**, 73–114.

6. Beland,F.A. and Kadlubar,F.F. (1990). In Cooper,C.S. and Grover,P.L. (eds), *Handbook of Experimental Pharmacology*, Springer-Verlag, Heidelberg, pp. 267–325.
7. Shibutani,S., Suzuki,N., Tan,X., Johnson,F. and Grollman,A.P. (2001) Influence of flanking sequence context on the mutagenicity of acetylaminofluorene-derived DNA adducts in mammalian cells. *Biochemistry*, **27**, 3717–3722.
8. Seo,K.Y., Jelinsky,S.A. and Loechler,E.L. (2000) Factors that influence the mutagenic patterns of DNA adducts from chemical carcinogens. *Mutat. Res.*, **463**, 215–246.
9. Patel,D.J., Mao,B., Gu,Z., Hingerty,B.E., Gorin,A., Basu,A.K. and Broyde,S. (1998) Nuclear magnetic resonance solution structures of covalent aromatic amine-DNA adducts and their mutagenic relevance. *Chem. Res. Toxicol.*, **11**, 391–407.
10. Cho,B.P. (2004) Dynamic conformational heterogeneities of carcinogen-DNA adducts and their mutagenic relevance. *J. Environ. Sci. Health. Part C-Environ. Carcinogen. Ecotoxicol. Rev.*, **22**, 57–90.
11. Meneni,S.R., D'Mello,R., Norigian,G., Baker,G., Gao,L., Chiarelli,M.P. and Cho,B.P. (2006) Sequence effects of aminofluorene-modified DNA duplexes: thermodynamic and circular dichroism properties. *Nucleic Acids Res.*, **34**, 755–763.
12. Meneni,S., Shell,S.M., Zou,Y. and Cho,B.P. (2007) Conformation-specific recognition of carcinogen-DNA adduct in E. coli. nucleotide excision repair. *Chem. Res. Toxicol.*, **20**, 6–10.
13. Meneni,S.R., Shell,S.M., Gao,L., Jurecka,P., Lee,W., Sponer,J., Zou,Y., Chiarelli,M.P. and Cho,B.P. (2007) Spectroscopic and theoretical insights into sequence effects of aminofluorene-induced conformational heterogeneity and nucleotide excision repair. *Biochemistry*, **46**, 11263–11278.
14. Brown,K., Hingerty,B.E., Guenther,E.A., Krishnan,V.V., Broyde,S., Turteltaub,K.W. and Cosman,M. (2001) Solution structure of the 2-amino-1- methyl-6-phenylimidazo[4,5-b]pyridine C8-deoxyguanosine adduct in duplex DNA. *Proc. Natl Acad. Sci. USA*, **98**, 8507–8512.
15. Mao,B., Vyas,R.R., Hingerty,B.E., Broyde,S., Basu,A.K. and Patel,D.J. (1996) Solution conformation of the N-(deoxyguanosin-8-yl)-1-aminopyrene ([AP]dG) adduct opposite dC in a DNA duplex. *Biochemistry*, **35**, 12659–12670.
16. Gu,Z., Gorin,A., Krishnasamy,R., Hingerty,B.E., Basu,A.K., Broyde,S. and Patel,D.J. (1999) Solution structure of the N-(deoxyguanosin-8-yl)-1-aminopyrene ([AP]dG) adduct opposite dA in a DNA duplex. *Biochemistry*, **38**, 10843–10854.
17. Cho,B.P., Beland,F.A. and Marques,M.M. (1992) NMR structural studies of a 15-mer DNA sequence from a ras protooncogene, modified at the first base of codon 61 with the carcinogen 4-aminobiphenyl. *Biochemistry*, **31**, 9587–9602.
18. Norman,D., Abuaf,P., Hingerty,B.E., Live,D., Grunberger,D., Broyde,S. and Patel,D.J. (1989) NMR and computational characterization of the N-(deoxyguanosin-8-yl)aminofluorene adduct [(AF)G] opposite adenosine in DNA: (AF)G[syn].A[anti] pair formation and its pH dependence. *Biochemistry*, **28**, 7462–7476.
19. Shapiro,R., Hingerty,B.E. and Broyde,S. (1989) Minor-groove binding models for acetylaminofluorene modified DNA. *J. Biomol. Struct. Dyn.*, **7**, 493–513.
20. Abuaf,P., Hingerty,B.E., Broyde,S. and Grunberger,D. (1995) Solution conformation of the N-(deoxyguanosin-8-yl)aminofluorene adduct opposite deoxyinosine and deoxyguanosine in DNA by NMR and computational characterization. *Chem. Res. Toxicol.*, **8**, 369–378.
21. Hingerty,B.E. and Broyde,S. (1990) Atomic resolution structures of DNA and DNA modified by carcinogens. *Internat. J. Supercomp. Appl.*, **4**, 11–21.
22. Elmquist,C.E., Wang,F., Stover,J.S., Stone,M.P. and Rizzo,C.J. (2007) Conformational differences of the C8-Deoxyguanosine adduct of 2-amino-3-methylimidazo[4,5-f]quinoline (IQ) within the *Nar*I recognition sequence. *Chem. Res. Toxicol.*, **20**, 445–454.
23. Wang,F., DeMuro,N.E., Elmquist,C.E., Stover,J.S., Rizzo,C.J. and Stone,M.P. (2006) Base-displaced intercalated structure of the food mutagen 2-amino-3-methylimidazo[4,5-f]-quinoline in the recognition sequence of the *Nar*I restriction enzyme, a hotspot for -2 bp deletions,. *J. Am. Chem. Soc.*, **128**, 10085–10095.
24. Wang,F., Elmquist,C.E., Stover,J.S., Rizzo,C.J. and Stone,M.P. (2007) DNA sequence modulates the conformation of the food mutagen 2-amino-3-methylimidazo[4,5-f]quinoline in the recognition sequence of the *Nar*I restriction enzyme. *Biochemistry*, **46**, 8498–8516.
25. Zaliznyak,T., Bonala,R., Johnson,F. and de Los Santos,C. (2006) Structure and stability of duplex DNA containing the 3-(deoxyguanosin-N^2-yl)-2-acetylaminofluorene (dG(N2)-AAF) lesion: a bulky adduct that persists in cellular DNA. *Chem. Res. Toxicol.*, **19**, 745–752.
26. Meneni,S.R., Liang,F. and Cho,B.P. (2007) Examination of the long-range effects of aminofluorene-induced conformational heterogeneity and its relevance to the mechanisms of translesion DNA synthesis. *J. Mol. Biol.*, **366**, 1387–1400.
27. Liang,F., Meneni,S.R. and Cho,B.P. (2006) Induced circular dichroism characteristics as conformational probes for carcinogenic aminofluorene-DNA adducts. *Chem. Res. Toxicol.*, **19**, 1040–1043.
28. Jain,N., Li,Y., Zhang,L., Meneni,S.R. and Cho,B.P. (2007) Probing the sequence effects on NarI-induced -2 frameshift mutagenesis by dynamic ^{19}F NMR, UV and CD spectroscopy. *Biochemistry*, **46**, 13310–13321.
29. Liang,F. and Cho,B.P. (2007) Probing the thermodynamics of aminofluorene-induced trans-lesion DNA synthesis by differential scanning calorimetry. *J. Am. Chem. Soc.*, **129**, 12108–12109.
30. Minetti,A.A., Remeta,D., Miller,H., Gelfand,C.A., Plum,G.E., Grollman,A.P. and Breslauer,K.J. (2003) The thermodynamics of template-directed DNA synthesis: base insertion and extension enthalpies. *Proc. Natl Acad. Sci. USA.*, **100**, 14719–14724.
31. Singer,B. and Hang,B. (2000) Nucleic acid sequence and repair: role of adduct, neighbor bases and enzyme specificity. *Carcinogenesis*, **21**, 1071–1078.
32. Zou,Y., Shell,S.M., Utzat,C.D., Luo,C., Yang,Z., Geacintov,N.E. and Basu,A.K. (2003) Effets of DNA adduct structure and sequence context on strand opening of repair intermediates and incision by UvrABC nuclease. *Biochemistry*, **42**, 12654–12661.
33. Ruan,Q., Liu,T., Kolbanovskiy,A., Liu,Y., Ren,J., Skovraga,M., Zou,Y., Lader,J., Malkani,B., Amin,S., Van Houten,B. and Geacintov,N.E. (2007) Sequence context- and temperature-dependent nucleotide excision repair of a benzo[a]pyrene diol epoxide-guanine DNA adduct catalyzed by thermophilic UvrABC proteins. *Biochemistry*, **46**, 7006–7015.
34. Cai,Y., Patel,D.J., Geacintov,N.E. and Broyde,S. (2007) Dynamics of a benzo[a]pyrene-derived guanine DNA lesion in TGT and CGC sequence contexts: enhanced mobility in TGT explains conformational heterogeneity, flexible bending, and greater susceptibility to nucleotide excision repair. *J. Mol. Biol.*, **374**, 292–305.
35. Kalam,M.A., Haraguchi,K, Chandani,S., Loechler,E.L., Moriya,M., Greenberg,M.M. and Basu,A.K. (2006) Genetic effects of oxidative DNA damages: comparative mutagenesis of the imidazole ring-opened formamidopyrimidines (Fapy lesions) and 8-oxo-purines in simian kidney cells. *Nucl. Acids Res.*, **34**, 2305–2315.
36. Kalam,M.A. and Basu,A.K. (2005) Mutagenesis of 8-oxoguanine adjacent to an abasic site in simian kidney cells: tandem mutations and enhancement of G→T transversions. *Chem. Res. Toxicol.*, **18**, 1187–1192.
37. Miller,H. and Grollman,A.P. (1997) Kinetics of DNA polymerase I (Klenow fragment exo-) activity on damaged DNA templates: effect of proximal and distal template damage on DNA synthesis. *Biochemistry*, **36**, 15336–15342.